Inextricable ties between chemical complexity and dynamics of embedded protostellar regions

Drozdovskaya, M.N.

5

THE ALMA-PILS SURVEY: THE SULFUR CONNECTION BETWEEN PROTOSTARS AND COMETS - IRAS 16293-2422 AND 67P/C-G

Maria N. Drozdovskaya, Ewine F. van Dishoeck, Jes K. Jørgensen,
Ursina Calmonte, Léna Le Roy, Kathrin Altwegg, PILS team
MNRAS, 2016b, in prep.

ABSTRACT

IRAS 16293-2422 is a one the most chemically rich low-mass protostellar system known to date and is likely one of the best Solar System analogues. ALMA Band 7 data from the large unbiased Protostellar Interferometric Line Survey (PILS) are searched for all sulfur-bearing molecules at the so-called "sweet spot" - a one beam offset position from source B. Species such as SO_2, OCS, CS, H_2CS and H_2S are either directly or indirectly detected via multiple isotopologues. Interferometric data permit spatial resolution of the emission and yields sufficient sensitivity to detect minor species. The search revealed a firm first-time detection of $OC^{33}S$ towards this source and a tentative first-time detection of $C^{36}S$ towards a low-mass protostar. A comparison in terms of molecular ratios with single dish observations reveals that single dish data are dominated by large scale outflow emission. Comets are thought to be the most pristine currently available tracers of the primitive Solar Nebula. Some of the best available data stemming from the ROSINA instrument aboard Rosetta are used to compare the sulfur budget of 67P/C-G with that of IRAS 16293-2422. Molecular ratios of 67P/C-G are shown to be significantly different from those towards the sweet spot with relatively more H_2S compared with OCS. This potentially indicates that our Solar System formed in a warmer, CO ice-poor environment that inhibits efficient OCS formation via grain-surface chemistry.

5.1 INTRODUCTION

Sulfur-bearing molecules have been detected in many interstellar environments from diffuse clouds to star-forming regions and rocky bodies in our Solar System. It is likely that the sulfur detected in cometary studies has its roots in the earliest diffuse phases of the interstellar medium. However, in comparison to diffuse clouds, observations show the total sulfur budget of dense cores to be depleted by several orders of magnitude. This puzzle remains unresolved and the missing sulfur is yet to be conclusively identified (e.g., Anderson et al. 2013). It has been postulated that sulfur may be a key element in linking the volatile and refractory components to a place of common origins, as it is found in both.

Some of the first detections of interstellar sulfur were in the gas phase towards Sgr B2 and Orion A in the 1970s - molecules such as CS, OCS, H_2S, SO, H_2CS and SO_2 were observed (Drdla et al., 1989; Jefferts et al., 1971; Minh et al., 1990; Pastor et al., 1991; Penzias et al., 1971). This also kicked off the studies of its chemistry, which suggested that in thin clouds sulfur is predominantly in the form of S^+ ions (Oppenheimer and Dalgarno, 1974) and likely undergoes partial incorporation into refractories. Meanwhile,

in dense clouds it is mostly neutral and gets incorporated into the observed volatiles via reactions with H_3^+ (Oppenheimer and Dalgarno, 1974) and grain-surface reactions (Duley et al., 1980). Subsequent chemical models quickly showed that the net sulfur budget as seen in volatiles is severely depleted in dense clouds (Prasad and Huntress, 1982). Some of the sulfur is incorporated into carbon chains such as CS, C_2S, C_3S and C_4S (Millar and Herbst, 1990; Smith et al., 1988; Wlodek et al., 1988). However, since the ionization potential of sulfur is lower than that of carbon, S^+ may exist in regions where most of carbon is neutral, which may lead to the formation of S_2 (suggested very early on by Duley et al. 1980). An important parameter is the initial elemental C/O ratio at time molecules start to form, which sets the ratio between oxygen- and carbon-containing S-bearing species (e.g., as seen in the ratio between SO and CS; Watt and Charnley 1985). Additional volatiles can be formed and/or enhanced via the passage of shocks, including HS, H_2S, S_2, SO^+ (Leen and Graff, 1988; Mitchell, 1984; Pineau des Forets et al., 1986; Turner, 1992). Species such as SO and SO_2 that are produced in the gas-phase via reactions with OH upon the liberation of S via sputtering, have become traditional shock tracers. Sulfur-bearing molecules have also been used to study disks via CS (e.g., Blake et al. 1992; Hasegawa et al. 1984) and as tracers of the centrifugal barrier via SO (e.g., Sakai et al. 2014).

Sulfur-bearing species also exist in the solid phase; and OCS ice was the first to be detected (Aikawa et al., 2012; Palumbo et al., 1995, 1997). Thereafter, the detection of solid SO_2 followed, but H_2S ice remains undetected (Boogert et al., 1997, 2015). The possible formation routes in ices towards species such as S_2 have already been investigated since Grim and Greenberg, (1987). In their experiments, ice mixtures containing H_2S are irradiated via ultraviolet (UV) photons and the production of sulfur chains is indirectly inferred. More recently, Chen et al., (2015) have shown energetic processing with UV of H_2S-CO ice mixtures leads to the formation of OCS and CS_2; and of H_2S-CO_2 mixtures to OCS and SO_2. It is thought that H_2S forms via the hydrogenation of atomic S and serves as a parent species for further synthesis of sulfur-bearing ices. It is suggested that SO forms on grain surfaces via oxygen addition to HS, and SO_2 forms via oxygen addition to SO and/or via the association of two SO molecules. OCS can potentially form via the addition of oxygen to CS, the addition of sulfur to CO and/or the association of HS and CO. Experiments also predict that H_2S_2 should be made on the grains via the association of two HS molecules. Further evidence on grain-surface chemistry of sulfur-bearing species is hidden in sulfur-bearing complex organics. The S-containing methanol analog, CH_3SH, has been detected towards the cold core B1 (Cernicharo et al., 2012); the hot core G327.3-0.6 (Gibb et al., 2000); Orion KL (Kolesniková et al., 2014); the O-type protostar IRAS 16547-4247 (Zapata et al., 2015); Sgr B2(N2) (Linke et al., 1979) and in the EMoCA survey (Müller et al., 2016). The S-containing ethanol analog, C_2H_5SH, has only been detected towards Orion KL; while searches towards Sgr B2(N2) remain uncertain (Müller et al., 2016). The network of sulfur chemistry on grain surfaces remains to be verified with detailed models and observations.

Sulfur-bearing species have also been detected in numerous places in the Solar System and several comets. A large reservoir of sulfur is found on Jupiter's moon Io, which has an atmosphere dominated by SO_2, as a result of active volcanic eruptions (e.g., Jessup et al. 2007). Contrary to the ISM, the majority of cometary detections of sulfur-bearing molecules belong to H_2S and S_2 (Ahearn et al., 1983; Mumma and Charnley, 2011). Only towards the brightest comet Hale-Bopp has a greater diversity been observed, including OCS, SO_2 and H_2CS. Currently, some of the most unique data to date are streaming in

from the *Rosetta* mission on comet 67P/Churyumov-Gerasimenko (67P/C-G hereafter). With the ROSINA instrument aboard the orbiter, the coma has been shown to contain H_2S, OCS, SO, SO_2, CS_2 and S_2 (and tentatively CS, as the mass spectrometer cannot distinguish it from CO_2) gases (Le Roy et al., 2015). Furthermore, S_3, S_4, CH_3SH, and C_2H_6S have now been detected (Calmonte et al., 2016, subm.) and information on isotopologues will be available soon (Calmonte et al. in prep.) It remains to be understood why surface sniffing of 67P/C-G by COSAC did not reveal any sulfur-bearing species (Goesmann et al., 2015). By piecing together the sulfur puzzle from the earliest diffuse phases to the oldest cometary probes, it may be possible to disentangle the history of volatiles and refractories simultaneously, as they are formed and assembled into larger bodies.

In this work, the sulfur trail is analyzed from the stance of the sulfur budget towards a low-mass protostar and how it compares to that of 67P/C-G, as unraveled by the ROSINA team. IRAS 16293-2422 is an embedded low-mass protostellar binary (Class 0/I) with a separation of 5.1″ or 620 AU (assuming a distance of 120 pc) and a combined luminosity of 21 ± 5 $L_\odot$. The system is associated with one collimated pair of outflow lobes in the NE-SW direction and one less collimated in the E-W direction. A full overview of the physical and chemical properties of the source are presented in Jorgensen et al. (2016, under rev.). There is a clear chemical differentiation between the A and B sources. Source A is significantly richer in sulfur-bearing species, as revealed with earlier interferometric studies (Jørgensen et al., 2011). Furthermore, the spatial distribution of the molecules varies, for example, CS is present on large scales in the envelope. The single dish survey with the CSO and JCMT telescopes detected CS, $C^{34}S$, SO, ^{34}SO, $S^{18}O$, SO, SiS, ^{29}SiS, HCS^+, OCS, $OC^{34}S$, $O^{13}CS$, ^{18}OCS, H_2S, HDS, o- and p-H_2CS, $H_2C^{34}S$, $H_2^{13}CS$, SO_2 (Blake et al. 1994; Dishoeck et al. 1995a and reanalyzed by Schöier et al. 2002), while the single dish TIMASSS survey with IRAM-30 m and JCMT-15 m facilities expanded the list with $^{34}SO_2$, ^{13}CS, $C^{33}S$, HDCS and C_2S (Caux et al., 2011). Interferometric observations with the SMA revealed the spatial distribution of CS, H_2CS, OCS, ^{33}SO, $^{33}SO_2$, $SO^{17}O$, ^{13}CS, $H_2C^{34}S$, $O^{13}CS$, ^{34}SO and $^{34}SO_2$ around the binary system (Jørgensen et al., 2011). IRAS 16293-2422 has been targeted with ALMA in Band 9 in terms of $^{34}SO_2$, $^{33}SO_2$ and SO (Baryshev et al., 2015).

This paper presents the full inventory of sulfur-bearing molecules towards IRAS 16293-2422, based on ALMA Band 7 data (Jorgensen et al. 2016, under rev.). Such interferometric observations make it possible to get away from the large scale outflow-dominated emission and spatially resolve the thermally desorbed molecules close to the central source. Subsequently, ratios between various molecules are compared to those deduced for the coma gases of 67P/C-G, as measured with the ROSINA instrument (Calmonte et al., 2016, subm.). Both sets of data are some of the best available for an extrasolar analogue of our Solar System and an innate Solar Nebula tracer - a comet. The differences and similarities between the two have implications for the formation history of our Solar System. Observational details are presented in Section 5.2 and the results are found in Section 5.3. Abundance ratios are computed and compared to cometary values in Section 5.4 and the conclusions are given in Section 5.5.

5.2 IRAS 16293-2422 OBSERVATIONS

This work is based on the large unbiased Protostellar Interferometric Line Survey (PILS; project-id: 2013.1.00278.S, PI: Jes K. Jørgensen) of IRAS 16293-2422 carried out with

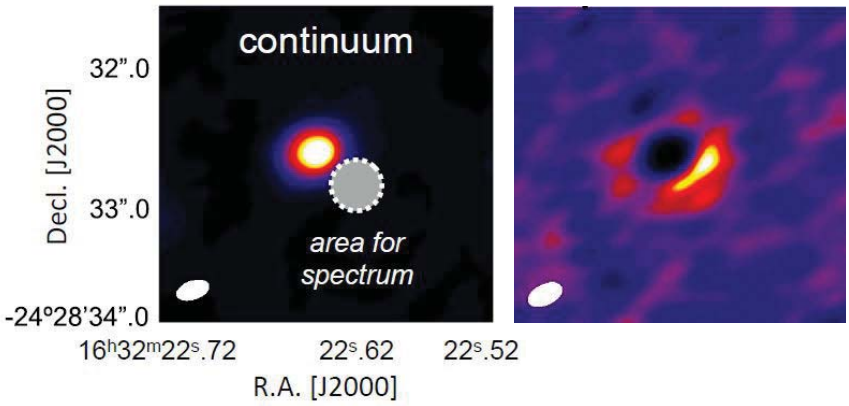

Figure 5.1: Left: ALMA Band 9 image at 690 GHz of IRAS 16293-2422 B from Baryshev et al., (2015). The circle indicates a 0.3″ beam used to extract the Band 9 spectrum shown in that paper. This position is close to the "sweet spot" used in this paper to extract the Band 7 spectrum in a 0.5″ beam by Jørgensen et al. (2016, under rev.). Right: Image of the $^{34}SO_2$ line near 686.6 GHz presented in Baryshev et al., (2015) showing the peak emission near the "sweet spot". Towards the strong continuum source itself, many lines are in absorption.

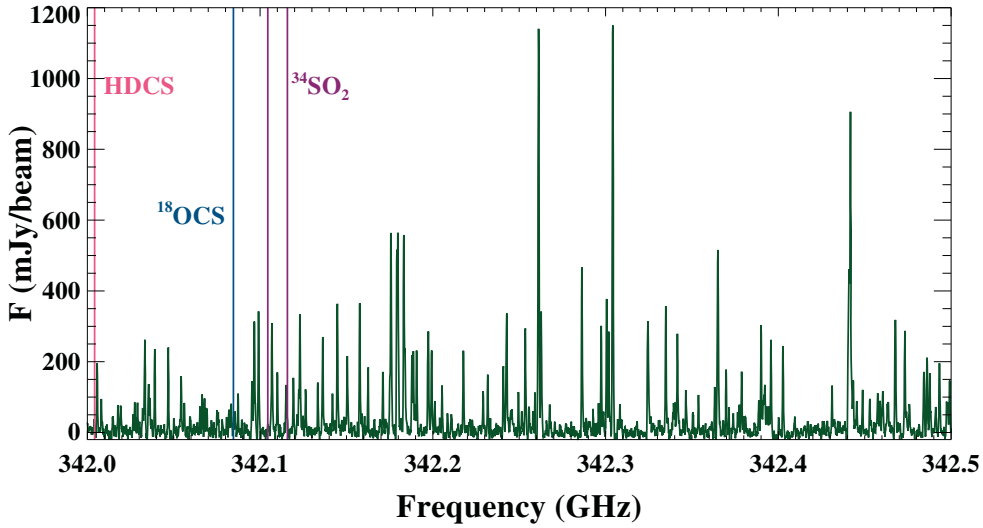

Figure 5.2: A section of the ALMA Band 7 spectrum at the "sweet spot" position illustrating the richness of the spectrum. The lines of some detected sulfur-bearing species that fall in this range are also shown.

ALMA in the $329 - 363$ GHz frequency range (Band 7) with a spectral resolution of 0.2 km s^{-1} and a beam size of $0.5''$ (or 60 AU in diameter, assuming a distance of 120 pc for the source). The local standard of rest (LSR) velocities assumed are 3.1 and 2.7 km s^{-1} for sources A and B, respectively. The data used here are continuum subtracted (based on the statistical method described in Jørgensen et al., 2016, under rev.) and are version 1.2 of the reduced dataset. The observations are a combination of the 12 and the 7 m dish arrays, thereby ensuring that the emission on large scales is recovered, while also spatially resolving the target. The root-mean-square (RMS) noise of the combined dataset is $\sim 7 - 10$ mJy beam^{-1} channel^{-1} (or $\sim 4 - 5$ mJy beam^{-1} km s^{-1} with beam sizes in the $\sim 0.4 - 0.7''$ range). Here, the dataset convolved with a uniform circular restoring beam of $0.5''$ is used. All further details on the PILS survey are available in Jørgensen et al. (2016, under rev.).

The spectral analysis presented in the subsequent section is carried out towards a single position of the dataset - one beam ($\sim$ 60 AU) offset from source B in the E direction (also called the "sweet spot"), which has also been the focal point of Coutens et al., (2016) and Lykke et al. (2016, subm.; twice as far as the position studied in Jørgensen et al. (2016, under rev.) in the same direction). The position is chosen to maximize emission at the higher densities that are on-source towards source B, while being sufficiently far from the source to avoid absorption against the strong dust continuum (Fig. 5.1; as seen in the Band 9 image in fig. 13 of Baryshev et al. 2015). The point also lies in the most outflow-free direction of the region to avoid any additional sources of heating. The spectrum at this "sweet spot" is rich in numerous lines from various species, as illustrated in Fig. 5.2. The recent analysis of complex organic emission in this direction from species such as glycolaldehyde, ethylene glycol, ethylene oxide, acetone and propanal indicate that the temperatures at this point are > 100 K, thus it is likely that the chosen position is probing hot inner envelope or face-on disk material heated by the protostellar B source. The choice to focus on source B has been made as its lines are much narrower than those observed towards source A, hence there is less line confusion and blending.

5.3 RESULTS

The one beam offset position (the "sweet spot") from source B of IRAS 16293-2422 in the PILS Band 7 dataset was searched for lines of all known sulfur-bearing species, especially those detected in 67P/C-G, and several that have been hypothesized to be present. The initial line searching and local thermal equilibrium (LTE) modeling have been carried out with CASSIS[2]. Thereafter, synthetic spectra have been generated with custom IDL routines. LTE is a good assumption in this case, because the densities are high at the chosen position and thus the molecules are expected to be thermalised. The detected species and the best-fitting parameters, assuming a constant $T_{ex} = 125$ K for all species, are tabulated in Table 5.1. This value for T_{ex} has been determined as best-fitting by eye based on a grid of synthetic spectra with 25 K steps. A value of 125 K is in agreement with what has been derived for acetaldehyde, ethylene oxide and propanal (Lykke et al., 2016, subm.), but is approximately a factor of 2 lower than the value of 300 K that has been derived for glycolaldehyde and ethylene glycol (Jørgensen et al., 2016, under rev.; however for a closer half beam offset position in the same direction) and isotopologues of formamide and isocyanic acid (Coutens et al., 2016). A constant source size of $0.5''$ (i.e., assuming that the emitting region equals the beam size) and a full width half-

2 CASSIS has been developed by IRAP-UPS/CNRS, http://cassis.irap.omp.eu

Table 5.1: Best-fitting parameters for detected species at the one beam offset position from source B of IRAS 16293-2422[a]

Species	# of clean lines (# of lines in range)	E_{up} (K)	N (cm^{-2})
SO_2, $v = 0$	13 (101)	$43 - 276$	1.5×10^{15}
$^{34}SO_2$	12 (107)	$35 - 185$	$4.0 \times 10^{14} \longrightarrow N(SO_2) = 5.9 \times 10^{15,e}$
SO, $v = 0$	0 (8)	$81 - 87$	$\leqslant 5.0 \times 10^{14,b}$
OCS, $v = 0$	0 (2)	$237 - 254$	$\geqslant 2.0 \times 10^{16,c}$
OCS, $v_2 = 1$	4 (4)	$986 - 1003$	2.0×10^{17}
$O^{13}CS$	2 (2)	$236 - 253$	$5.0 \times 10^{15} \longrightarrow N(OCS) = 3.5 \times 10^{17,d}$
$OC^{34}S$	3 (3)	$231 - 265$	$1.5 \times 10^{16} \longrightarrow N(OCS) = 3.3 \times 10^{17,e}$
$OC^{33}S$	2 (3)	$234 - 268$	$3.0 \times 10^{15} \longrightarrow N(OCS) = 3.8 \times 10^{17,f}$
^{18}OCS	3 (3)	$238 - 272$	$7.0 \times 10^{14} \longrightarrow N(OCS) = 3.9 \times 10^{17,g}$
$C^{34}S$, $v = 0, 1$	1 (2)	65	$3.0 \times 10^{14} \longrightarrow N(CS) = 6.6 \times 10^{15,e}$
$C^{33}S$, $v = 0, 1$	0 (2)	65	$\leqslant 1.0 \times 10^{14,b} \longrightarrow N(CS) \leqslant 1.3 \times 10^{16,f}$
$C^{36}S$	1 (1)	64	$2.0 \times 10^{13} \longrightarrow N(CS) = 9.5 \times 10^{16,h}$
H_2CS	9 (22)	$102 - 419$	1.5×10^{15}
HDCS	6 (23)	$98 - 322$	$1.5 \times 10^{14} \longrightarrow N(H_2CS) = = 1.5 \times 10^{15,i} - 1.5 \times 10^{16,j}$
HDS	1 (10)	35	$2.0 \times 10^{16} \longrightarrow N(H_2S) = = 2.0 \times 10^{17,i} - 2.0 \times 10^{18,j}$
$HD^{34}S$	1 (7)	35	$1.0 \times 10^{15} \longrightarrow N(HDS) = = 2.2 \times 10^{16,e} \longrightarrow N(H_2S) = = 2.2 \times 10^{17,i} - 2.2 \times 10^{18,j}$

[a] assuming a source size of 0.5″, FWHM of 1 km s^{-1} and $T_{ex} = 125$ K

[b] blended

[c] optically thick

[d] assuming $^{12}C/^{13}C = 70$

[e] assuming $^{32}S/^{34}S = 22$

[f] no estimate for local ISM is available, so a solar ratio of $^{32}S/^{33}S = 125$ is used

[g] assuming $^{16}O/^{18}O = 560$

[h] no estimate for local ISM is available, so a solar ratio of $^{32}S/^{36}S = 4747$ is used

[i] assuming D/H= 0.1, as measured with single-dish observations in HDS/H_2S (table 11 of Dishoeck et al. 1995a)

[j] assuming D/H= 0.01, as recent studies suggest that single dish observations may be overestimating deuteration as a result of underestimating optical depth

maximum (FWHM) of 1 km s^{-1} are assumed. Subsequent subsections describe the details of the detections on a molecule by molecule basis. Isotope ratios for the local interstellar medium (ISM) have been taken from Wilson and Rood, (1994) where available. Otherwise, solar ratios from Asplund et al., (2009) have been employed. A selection of the detected lines and fitted synthetic spectra are available as tables and figures in Appendix 5.7.

5.3.1 *SO_2*

Sulfur dioxide (SO_2) in the $v = 0$ state (CDMS entry 64502) has 101 lines in range of the PILS Band 7 dataset and 13 have been detected in a clean non-blended manner (with upper energy levels, E_u, up to 276 K and Einstein A coefficients $\geqslant 1.2 \times 10^{-4}$). The rest are blended with lines from the many other molecules emitting at this position. The best fitting column density is 1.5×10^{15} cm^{-2}. In the $v_2 = 1$ state (CDMS entry 64503), 83 lines are in range; but only 1 is detected cleanly, since all these lines have very high upper energy levels ($E_u \gtrsim 800$ K) and thus are not expected to be strong. In addition, 107 lines of $^{34}SO_2$ (CDMS entry 66501) are in range and 12 are detected cleanly (with $E_u < 185$ K and Einstein A coefficients $\geqslant 4.35 \times 10^{-5}$). The best fitting column density is 4.0×10^{14} cm^{-2}. For a ratio of $^{32}S/^{34}S = 22$, the column density of SO_2 should be 5.9×10^{15} cm^{-2}, which is no more than a factor of ~ 6 higher than the column density derived from the lines of SO_2 itself. The one beam offset position has also been searched for $^{33}SO_2$ (CDMS entry 65501, 471 lines in range), $S^{18}OO$ (CDMS entry 66502, 169 lines in range) and $S^{17}OO$ (CDMS entry 65502, 137 lines in range); however, all these lines are very weak and lie at most at the noise level of the dataset.

5.3.2 *SO*

Sulfur monoxide (SO) in the $v = 0$ state (CDMS entry 48501) has 8 lines in range. Only 2 are strong enough to be detected and are unfortunately blended with emission from C_3H_2 and C_2H_3CN. Therefore, the LTE fit for this molecule is less certain and only an upper limit can be derived on its column density at a value of 5.0×10^{14} cm^{-2}. This value reflects the maximal contribution SO can have in the observed blended lines. In the $v = 1$ state (CDMS entry 48502), 7 lines are in range, but all are predicted to be weaker than 1 mJy $beam^{-1}$ and are thus under the noise level of the dataset. The position has also been searched for ^{34}SO (CDMS entry 50501, 6 lines in range), ^{33}SO (CDMS entry 49501, 45 lines in range), ^{36}SO (CDMS entry 52502, 6 lines in range), $S^{18}O$ (CDMS entry 50502, 7 lines in range), $S^{17}O$ (CDMS entry 49502, 52 lines in range) and SO^+ (CDMS entry 48010, 2 lines in range); however, all these lines are very weak and are not detected above the noise level of the dataset.

5.3.3 *OCS*

Carbonyl sulfide (OCS) in the $v = 0$ state (CDMS entry 60503) has 2 lines in range ($E_u < 254$ K and Einstein A coefficients $\geqslant 1.15 \times 10^{-4}$); however, both are blended with lines from glycolaldehyde and ethanol. In the $v_2 = 1$ state, there are 4 lines in range, which are all cleanly detected ($E_u < 1003$ K and Einstein A coefficients $\geqslant 1.12 \times 10^{-4}$). Multiple isotopologues have also been detected: $O^{13}CS$ (CDMS entry 61502) with 2 clean lines in range ($E_u < 253$ K and Einstein A coefficients $\geqslant 1.14 \times 10^{-4}$); $OC^{34}S$

(CDMS entry 62505) with 3 clean lines in range ($E_u < 265$ K and Einstein A coefficients $\geqslant 1.07 \times 10^{-4}$); $OC^{33}S$ (CDMS entry 61503) with 3 lines in range and 2 cleanly detected ($E_u < 268$ K and Einstein A coefficients $\geqslant 1.11 \times 10^{-4}$); ^{18}OCS (CDMS entry 62506) with 3 lines in range and all cleanly detected ($E_u < 272$ K and Einstein A coefficients $\geqslant 1.06 \times 10^{-4}$). This is the first time $OC^{33}S$ has been detected towards this source. The presence of ^{33}S has been inferred previously via $^{33}SO_2$ (Jørgensen et al., 2012) and $C^{33}S$ (Caux et al., 2011). All the other isotopologues of OCS have been detected previously (Blake et al., 1994; Caux et al., 2011; Schöier et al., 2002). The dataset was also searched for ^{17}OCS (CDMS entry 61504), $OC^{36}S$ (CDMS entry 64510), $^{18}OC^{34}S$ (CDMS entry 64511), $^{18}O^{13}CS$ (CDMS entry 63503), $O^{13}C^{34}S$ (CDMS entry 63502), $O^{13}C^{33}S$ (CDMS entry 62507); however, the emission from these species is at the noise level of the dataset.

The best-fitting column density of OCS is 2.0×10^{17} cm^{-2} if inferred from the 4 lines of the $v_2 = 1$ state and is 2.0×10^{16} cm^{-2} if approximated from the 2 (blended) lines of the $v = 0$ state, but lines with this state are optically thick. Alternatively, its column density can be inferred indirectly via its optically thin isotopologues: based on $O^{13}CS$ and assuming that $^{12}C/^{13}C = 70$, the column density should be 3.5×10^{17} cm^{-2}; based on $OC^{34}S$ and assuming that $^{32}S/^{34}S = 22$, the column density should be 3.3×10^{17} cm^{-2}; and based on ^{18}OCS and assuming that $^{16}O/^{18}O = 560$, the column density should be 3.9×10^{17} cm^{-2}. These values agree within 30% and are within a factor two from the column density calculated from the $v_2 = 1$ state and a factor of 10 higher than that based on the $v = 0$ state confirming the optical thickness. The average of these 4 values is 3.2×10^{17} cm^{-2}. The average of the values based on the 3 isotopologues is 3.6×10^{17} cm^{-2} and is the best estimate of the column density of OCS at this position. As an additional check, the solar ratio of $^{32}S/^{33}S = 125$ can be used to derive the column density of OCS from its $OC^{33}S$ isotopologue, since no estimate for the local ISM is available. This yields a value of 3.8×10^{17} cm^{-2}, which is consistent with the average value derived from three other isotopologues.

5.3.4 *CS*

Carbon monosulfide (CS) in the $v = 0-4$ state (CDMS entry 44501) has 5 lines in range. Only 1 of them in $v = 0$, $J = 7-6$, is expected to be strong enough to be detected ($E_u = 66$ K and Einstein A coefficient of 8.40×10^{-4}), unfortunately there is some self-absorption in the line, which makes it hard to derive a column density. The $C^{34}S$ isotopologue in the $v = 0, 1$ state (CDMS entry 46501) has 2 lines in range. One is cleanly detected, while the second is too weak to detect as $E_u \sim 1880$ K. The best fitting column density is 3.0×10^{14} cm^{-2}. The $C^{33}S$ isotopologue in the $v = 0, 1$ (CDMS entry 45502) also has 2 lines in range. One is cleanly detected, while the second is again too weak to detect as $E_u \sim 1887$ K. The best fitting column density is 1.0×10^{14} cm^{-2}. The fourth S-isotopologue $C^{36}S$ (CDMS entry 48503) has 1 line in range and it is cleanly detected ($E_u = 64$ K and Einstein A coefficient of 7.66×10^{-4}), giving a best fitting column density 2×10^{13} cm^{-2}. This is the first time detection of ^{36}S towards a low-mass protostar. $C^{36}S$ has been previously detected towards high-mass hot cores (Mauersberger et al., 1996) as a first-time detection of interstellar ^{36}S. More lines are required to fully secure this detection; however, the isotopic ratios are in agreement with solar ratios. Other excitation states and isotopologues lack lines in the observed frequency range, specifically: CS in the $v = 1-0, 2-1$ (CDMS entry 44510) and $v = 2-0$ (CDMS entry 44511) states; $C^{34}S$ in the $v = 1-0$ state (CDMS entry 46510); ^{13}CS in the $v = 0, 1$ and $v = 1-0$ states

(CDMS entries 45501 and 45509); $^{13}C^{34}S$ (CDMS entry 47501) and $^{13}C^{33}S$ (CDMS entry 47501). Meanwhile, $^{13}C^{36}S$ (CDMS entry 49508) has 1 line in range, but it is a clear non-detection.

Assuming the local ISM ratio of $^{32}S/^{34}S = 22$ (Wilson and Rood, 1994), the column density of CS can be estimated at 6.6×10^{15} cm^{-2} from its $C^{34}S$ isotopologue. If this column density is used to fit the detected line of CS suffering from absorption, then the line width is consistent with the value derived from $C^{34}S$. Thus this is the best available estimate of the column density of CS. Again as an additional check, the solar ratio of $^{32}S/^{33}S = 125$ can be used to derive the upper limit on the column density of CS from its $C^{33}S$ isotopologue. This yields a value of 1.3×10^{16} cm^{-2}, which is consistent with the value derived from $C^{34}S$. Furthermore, the solar ratio of $^{32}S/^{36}S = 4747$ can be used to derive the column density of CS from its $C^{36}S$ isotopologue, since no estimate for the local ISM is available. This yields a value of 9.5×10^{16} cm^{-2}, which is only a factor of 1.4 larger than the value derived from $C^{34}S$.

5.3.5 *H_2CS*

Thioformaldehyde (H_2CS; CDMS entry 46509) has 22 lines in range and 9 are cleanly detected ($E_u < 419$ K and Einstein A coefficients $\geqslant 4.57 \times 10^{-4}$. The best fitting column density is 1.5×10^{15} cm^{-2}. In addition, its isotopologue HDCS (CDMS entry 47504) has 23 lines in range, of which 6 are detected cleanly ($E_u < 322$ K and Einstein A coefficients $\geqslant 4.74 \times 10^{-4}$. The best fitting column density is 1.5×10^{14} cm^{-2}. Assuming $D/H = 0.1$, as measured with single-dish observations in HDS/H_2S (table 11 of Dishoeck et al. 1995a), yields a column density of 1.5×10^{15} cm^{-2} for H_2CS, which is in exact agreement with the column density derived based on its own lines. However, recent studies suggest that single dish observations may be overestimating deuteration, either because of sampling colder material or as a result of underestimating optical thickness of the main species (Coutens et al. 2016, Jørgensen et al. 2016, under rev., Persson et al. 2016, in prep.). Thus, if $D/H = 0.01$ is assumed, as typically found in PILS data of other molecules, then the column density of H_2CS may be as high as 1.5×10^{16} cm^{-2}. Other isotopologues have not been detected: $H_2C^{34}S$, $H_2C^{33}S$ and $H_2^{13}CS$ (CDMS entries 48508, 47506 and 47505).

5.3.6 *H_2S*

Hydrogen sulfide (H_2S; CDMS entry 34502) has 1 line in the observed frequency range, however it is a clear non-detection due to a high upper energy level ($E_u = 758$ K) and line weakness (Einstein A coefficient of 6.28×10^{-9}). On the other hand, its isotopologue HDS (CDMS entry 35502) has 10 lines in range. One of those is a clear detection, while the others have upper energy levels that are too high ($E_u > 537$ K) and thus are not expected to be strong. The best-fitting column density is 2.0×10^{16} cm^{-2}. $HD^{34}S$ (CDMS entry 37503) has 7 lines in range. One is cleanly detected, while all others have upper energy levels that are too high ($E_u > 536$ K) to be strong. The best fitting column density is 1.0×10^{15} cm^{-2}. Assuming that $^{32}S/^{34}S = 22$, gives a column density of 2.2×10^{16} cm^{-2} for HDS, which closely agrees with the value derived based on its solo observed line. Other isotopologues are not detected. $H_2^{34}S$ and $H_2^{33}S$ do not have any lines in the observed frequency range (CDMS entries 36504 and 35503). D_2S (CDMS entry 36503) has 4 lines in range; however, only 2 are above the noise level and both

suffer from blending, thus no clear detection is available. $D_2\ ^{34}S$ (CDMS entry 38507) has 2 lines in range, but one is subject to strong absorption at that frequency and the other is blended with $C_2H_5\ ^{13}CN$; thus no confident detection can be claimed.

Assuming D/H= 0.1, as measured with single-dish observations in HDS/H_2S (table 11 of Dishoeck et al. 1995a), the column density of H_2S can be estimated at 2.0×10^{17} cm^{-2} from HDS and at 2.2×10^{17} cm^{-2} from $HD^{34}S$. The two values are in very close agreement and their average of 2.1×10^{17} cm^{-2} is our best estimate of the column density of H_2S at this position. If a ratio of D/H= 0.01 is assumed, as motivated above, then the best estimate increases to 2.1×10^{18} cm^{-2}.

The previously obtained SMA observations of IRAS 16293-2422 have detected a line of H_2S around ~ 216.71 GHz (see fig. 6 of Jørgensen et al. 2011). LTE modelling assuming a beam size of 3″, a spectral resolution of 0.56 km s^{-1} (as given in table 1 of Jørgensen et al. 2011), FWHM of 1 km s^{-1} and a source size of 0.5″ (as assumed for the ALMA observations) shows that the line is optically thick. In order to match the observed line intensity of ~ 2 Jy beam^{-1}, a larger source size is necessary. Upon the assumption of a source 1″ in size, the lower limit on the column density of H_2S is 4.0×10^{16} cm^{-2}. This illustrates the uncertainty in the emitting area of this molecule. Alternatively, a non-detection of the sole line in range of the SMA observations of $H_2^{34}S$ at ~ 226.70 GHz does not yield a strongly constraining column density estimate. Assuming the same parameters, then in order to be weaker than the 3σ noise level (where σ = 0.24 Jy beam−1 chan^{-1}; table 1 of Jørgensen et al. 2011), the column density of $H_2^{34}S$ must not exceed 4.0×10^{19} cm^{-2}. Assuming $^{32}S/^{34}S$= 22, the upper limit on the column density of H_2S is 8.8×10^{20} cm^{-2}. This is consistent with the limits obtained with the uncertain limit obtained from HDS, but is less constraining than the other. Dedicated high resolution ALMA observations are needed in order to constrain the spatial distribution and column density of H_2S.

5.3.7 *Other species*

Other species that were searched for and have lines in range of the dataset, but are not detected at this position include oxyhydroxysulfonium (cis-$HOSO^+$; CDMS entry 65510), sulfur chain species S_2, S_3, S_4 (JPL entries 64001, 96002, 128001), HS_2 (CDMS entry 65509), H_2S_2 (CDMS entry 66507), S_2O (CDMS entry 80503), cis-S_2O_2 (CDMS entry 96501), silicon monosulfide (SiS) and its isotopologues (CDMS entries 62508, 62509, 61508, 64514, 61506, 61507, 62510, 62511, 63504, 62512, 65507, 64513, 63505, 66505, 60506, 60507, 60508), HSiS (CDMS entry 61512), H_2SiS (CDMS entry 62513), OSiS (CDMS entry 76517), atomic S (CDMS entry 32511), $HOCS^+$ (CDMS entry 61510), $HSCO^+$ (CDMS entry 61509), t- and c-HC(O)SH (CDMS entries 62515 and 62516), SH^- (CDMS entry 33504), SH^+ (CDMS entry 33505), HSO (CDMS entry 49512), g- and a-C_2H_5SH (CDMS entries 62523 and 62524).

5.4 DISCUSSION

5.4.1 *Comparison with single dish observations*

The presented interferometric observations are capable of spatially resolving the hot inner regions near the continuum peak source B, which resolves issues such as beam dilution that plague single dish observations. Moreover, it is possible to detect weaker lines from multiple isotopologues, thereby allowing a better determination of the optical

Table 5.2: Abundance ratios relative to H_2S and OCS of IRAS 16293-2422 as measured with these interferometric ALMA observations and previous single dish work[k]

Species	N (cm^{-2})	Abundance ratio relative to H_2S (%)				Abundance ratio relative to OCS (%)			
		sweet spot[l]	constant	inner	outer	sweet spot[l]	constant	inner	outer
H_2S	$2.1 \times 10^{17,i} - 2.1 \times 10^{18,j}$	100	100	-	-	$58.3 - 583$	23	-	-
OCS	3.6×10^{17}	$171 - 17$	438	-	-	100	100	100	100
SO	5.0×10^{14}	$0.2 - 0.02$	275	-	-	0.14	63	100	117
SO_2	1.5×10^{15}	$0.7 - 0.07$	39	-	-	0.4	8.9	40	15
CS	6.6×10^{15}	$3.1 - 0.3$	188	-	-	1.8	43	-	-
H_2CS	1.5×10^{15}	$0.7 - 0.07$	13	-	-	0.4	3	1.2	3.3

[i,j] see footnotes of Table 5.1

[k] tables 5 and 6 of Schöier et al., (2002))

[l] one beam (~ 60 AU) offset from source B of IRAS 16293-2422 in the E direction

Table 5.3: Abundance ratios relative to H_2S and OCS of IRAS 16293-2422 in comparison to those of 67P/C-G[m]

Species	N (cm^{-2})	Abundance ratio relative to H_2S (%)		Abundance ratio relative to OCS (%)		
		sweet spot[l]	67P/C-G	sweet spot[l]	67P/C-G	W33A[n]
H_2S	$2.1 \times 10^{17,i} - 2.1 \times 10^{18,j}$	100	100	$58.3 - 583$	2257	$< 30 - 90$
OCS	3.6×10^{17}	$171 - 17$	4.43 ± 0.15	100	100	100
SO	5.0×10^{14}	$0.2 - 0.02$	7.06 ± 0.17	0.14	159	-
SO_2	1.5×10^{15}	$0.7 - 0.07$	12.5 ± 0.3	0.4	282	$3 - 7$
CS	6.6×10^{15}	$3.1 - 0.3$	-	1.8	-	-

[m] bulk coma ROSINA measurements corrected for photodissociation and ionization (table 3 of Calmonte et al., 2016, subm.)

[n] interstellar ice ratios for W33A - the strongest ice source; Boogert et al., (1997) and Tak et al., (2003)

depth. By comparing abundance ratios of interferometric and single dish observations, it is possible to disentangle whether molecules primarily emit on large scales or small inner scales near the source, or whether they are associated with outflows. For this purpose, Table 5.2 has been compiled with molecular ratios of the detected species relative to H_2S and OCS (where available), as obtained with the PILS survey with ALMA and with a compilation of single dish observations of (Schöier et al., 2002). Since single dish observations cannot spatially resolve the emission, three different sets of abundances are typically provided: one assuming a constant profile and one assuming a jump profile, giving an inner (hot) abundance and an outer (cold) one.

From Table 5.2 it can be seen that relative to H_2S the interferometric ratio for OCS is lower by a factor of $3-26$, for SO by $3-4$ orders of magnitude, and for SO_2, CS, and H_2CS by $2-3$ orders of magnitude than the ratio measured with single dish observations based on a constant abundance assumption. When measured relative to OCS, the interferometric ratio for H_2S is a factor of $2.5-25$ higher than the single dish value. Meanwhile, all other interferometric ratios are still lower: for SO by 3 orders of magnitude, for SO_2 by a factor of ~ 21, for CS by a factor of ~ 23 and for H_2CS by a factor ~ 7. When comparing relative to OCS with the inner and outer ratios, the differences are either comparable or exacerbated further. The inner ratio is expected to be most relevant as it is the closest estimate for the hot component. This implies that most of the emission from these sulfur-bearing species in single-dish measurements is dominated by large scales, i.e., those associated with outflows emanating from the source. This is in agreement with the largest differences being seen for SO - a well-known shock tracer that shows larger line widths in the single dish data.

The interferometric column density estimates for SO and SO_2 likely give limits on the maximal quantities of these species being produced via grain-surface reactions and then immediately thermally desorbed in the "sweet spot". However, SO and SO_2 can also be efficiently produced at high ($100\ K < T < 300\ K$) temperatures in the gas-phase via reactions of S and OH. OH is readily available at such high temperatures and seen in *Herschel* data (Wampfler et al., 2013). Single dish observations likely probe all these components at the same time due to the very large beam size. Furthermore, the position analysed in this work - the "sweet spot", is not the location with the strongest emission of sulfur-species. In fact, such species peak towards source A of IRAS 16293-2422, which powers stronger outflows in its vicinity. The analysis of a point near source A is the subject of future work. These will then also be compared with the results obtained by Oya et al., (2016), which suggest that OCS traces the infalling–rotating envelope, while H_2CS is associated with the centrifugal barrier of the disk and also with the envelope.

5.4.2 *Comparison with ROSINA data on 67P/C-G*

IRAS 16293-2422 is thought to be analogous to our innate Solar Nebula as it is one of the most chemically rich low-mass protostellar systems. Meanwhile, it has also been postulated that comets are the most pristine tracers of the protoplanetary disk that evolved into the Solar System that we have today. Therefore, it is interesting to compare the chemical inventories of comets to those of IRAS 16293-2422 in order to quantify the chemical budgets of Solar and extrasolar building blocks of planetary systems (Bockelée-Morvan et al., 2015; Schöier et al., 2002). The emission seen in the hot inner regions of this protostellar core could potentially be tracing solid species that are undergoing thermal desorption and thus is in fact probing the hidden solid reservoir of planet-building material.

Table 5.3 contains the abundance ratios relative to H_2S and OCS at the "sweet spot" of IRAS 16293-2422 in comparison to those of 67P/C-G, as obtained for the bulk coma with ROSINA measurements corrected for photodissociation and ionization (table 3 of Calmonte et al., 2016, subm.). It can be seen that for OCS the "sweet spot" ratio relative to H_2S is a factor of $\sim 3.8-39$ higher than that for 67P/C-G, for SO a factor of $\sim 3.5-35$ lower and for SO_2 a factor of $\sim 1.8-18$ lower. Relative to OCS the "sweet spot" ratio for H_2S is a factor of $\sim 3.9-39$ lower than that for 67P/C-G, for SO is ~ 3 orders of magnitude and for SO_2 is ~ 2 orders or magnitude lower. Such large differences are consistent with the fact that H_2S has not yet been detected in interstellar ices, but OCS has.

These results indicate that in the case of IRAS 16293-2422 there is significantly more OCS available, while for 67P/C-G more H_2S is present. Potentially, this has to be to do with the amount of solid carbon monoxide (CO) available in these systems. OCS is more easily produced via grain-surface chemistry when CO ice is abundant. CO undergoes thermal desorption into the gas-phase around 20 K and at that point the production of OCS is inhibited. Dedicated chemical models need to be run in order to quantify such effects. Nevertheless, this could be an initial indication of our Solar System being born in a somewhat warmer environment, i.e., > 20 K rather than in the $10-15$ K regime, which would lead to less CO being available on the grains for the synthesis of OCS. This scenario is also favored from the point of view of oxygen chemistry and the detection of O_2 on 67P/C-G (Bieler et al. 2015, Taquet et al., 2016, subm.). An enhanced availability of CO in the case of IRAS 16293-2422 is supported by the fact that the cold surrounding core is still observed in its current Class 0 phase. Such temperature differences should also be noticeable in terms of complex organics in these systems and the comparison in terms of sulfur-bearing and other complex organics are the topic of future publications.

Table 5.3 also contains the abundance ratios relative to OCS as observed towards W33A - the strongest ice source, which trace the interstellar ice content (Boogert et al., 1997; Tak et al., 2003). It is necessary to look towards the brightest available source in order to detect these trace species in the ISM ice, which is dominated by water ice. It can immediately be noted that for H_2S and SO_2, the ISM ice ratios relative to OCS are much closer to those of the "sweet spot" than for 67P/C-G. This could potentially be an indication that the 67P/C-G abundances are indeed indicating initial conditions that are different from those towards other protostellar sources.

Another stark difference between the IRAS 16293-2422 observations and 67P/C-G is that the former is shown to contain CS and H_2CS, both of which are not detected towards 67P/C-G. Both of these species have gas-phase routes to formation, as well as grain-surface pathways. Finally, the ROSINA team has also discovered sulfur chain fragments, such as S_2, S_3 and S_4 in their data on 67P/C-G (Calmonte et al., 2016, subm.). Such species have not been detected towards protostars and the search is ongoing (Martín-Doménech et al., 2016), as these species provide a link between the volatile sulfur-bearing molecules and the refractory component of cometary and protoplanetary materials.

5.4.3 *Comparison with models*

Efforts on chemical modelling of sulfur networks have recently been revived by Woods et al., (2015). The authors computed the abundances of sulfur-bearing species for hot core conditions upon the inclusion of recent experimental and theoretical data into their chemical network, including a refractory sulfur residue. The modelled abundance ratios

(relative to either H_2S or OCS; as tabulated in table 9 of Woods et al., (2015) for the standard model with the interstellar cosmic ray ionization rate of 1.3×10^{-17} s^{-1}) can be compared to those derived in this work for the "sweet spot" of IRAS 16293-2422 B. An agreement within one order of magnitude is found for OCS and CS, and the modelled ratios are in range of the observed "sweet spot" ratios for H_2S. The modelled ratios for H_2CS are three orders of magnitude higher, which maybe explained by the fact that the grain-surface network used in the models is fairly small and the grain-surface chemistry is not fully accounted for. H_2CS is expected to be involved in many grain-surface reactions and will likely be used up for synthesis of larger sulfur-bearing species, such as CH_3SH (analogous to the sequential hydrogenation of CO leading to CH_3OH with H_2CO as an intermediate).

The ratios for SO and SO_2 vary by many orders of magnitude between these observations and the models of Woods et al., (2015). This likely has to do with the fact that the models have been run for a very long time of 10^7 yr, which implies that many gaseous species are driven into SO and SO_2, leading to their overproduction. At earlier times (as seen in fig. 6 of Woods et al., (2015)), the model results have a closer agreement with observations of the "sweet spot" for SO. SO_2 remains too high nevertheless, which may have to do with thermal desorption being calculated via an efficiency factor. The development of a full gas-grain chemical network for sulfur, including grain-surface chemistry, is the topic of future research.

5.5 CONCLUSIONS

In this paper the sulfur inventory of the "sweet spot" in the vicinity of source B in the binary protostellar system IRAS 16293-2422 has been presented. The ALMA Band 7 data analyzed are part of the PILS survey towards this target. Sulfur is thought to be a unique simultaneous tracer of both the volatile and refractory components. By comparing molecular ratios observed towards IRAS 16293-2422 - a Solar System proxy, and those obtained for 67P/C-G - a most pristine available tracer of the innate Solar Nebula, the chemical links between the early embedded protostellar phases and the protoplanetary building blocks can be explored. The main conclusions of this paper are as follows:

1. The sulfur-bearing species previously detected towards IRAS 16293-2422 have now been firmly detected towards the "sweet spot" and spatially resolved with ALMA: SO_2 in the $v = 0$, $^{34}SO_2$, OCS in the $v_2 = 1$ state, $O^{13}CS$, $OC^{34}S$, $OC^{33}S$ (first-time detection towards this source), ^{18}OCS, H_2CS and HDCS. Furthermore, several are detected tentatively due to a lack of lines and/or blending: SO_2 in the $v_2 = 1$ state, SO in the $v = 0$ state, OCS in the $v = 0$ state, CS in the $v = 0 - 4$ state, $C^{34}S$, $C^{33}S$, $C^{36}S$ (tentative first time detection towards a low-mass protostar), HDS and $HD^{34}S$.

2. In comparison to earlier single dish observations, the molecular ratios determined from interferometric data can be several orders of magnitude lower. This implies that the single dish data are dominated by large scale outflow-dominated emission.

3. In comparison to ROSINA measurements of the coma gases of 67P/C-G, IRAS 16293-2422 molecular ratios differ significantly, potentially by as much as several orders of magnitude. In particular, IRAS 16293-2422 contains much more OCS than

H_2S, potentially indicating that our Solar System was born in a somewhat warmer ($T \sim 20$ K), CO ice-poor environment.

Future publications will explore the protostellar-cometary connection via isotopic ratios and a full set of complex organic species, thereby isolating chemical links formed during cold phases of evolution that are dominated by grain-surface chemistry.

5.6 ACKNOWLEDGEMENTS

The authors would like to thank Dr. Catherine Walsh, Dr. Vianney Taquet and Mr. Ko-Ju Chuang for useful discussions on sulfur chemistry. This work is supported by a Huygens fellowship from Leiden University, by the European Union A-ERC grant 291141 CHEMPLAN, by the Netherlands Research School for Astronomy (NOVA) and by a Royal Netherlands Academy of Arts and Sciences (KNAW) professor prize.

5.7 APPENDIX

A SELECTION OF LINES AND SYNTHETIC SPECTRA OF S-BEARING SPECIES IN THE PILS BAND 7 DATASET

Similar plots will follow for all the other detected molecules.

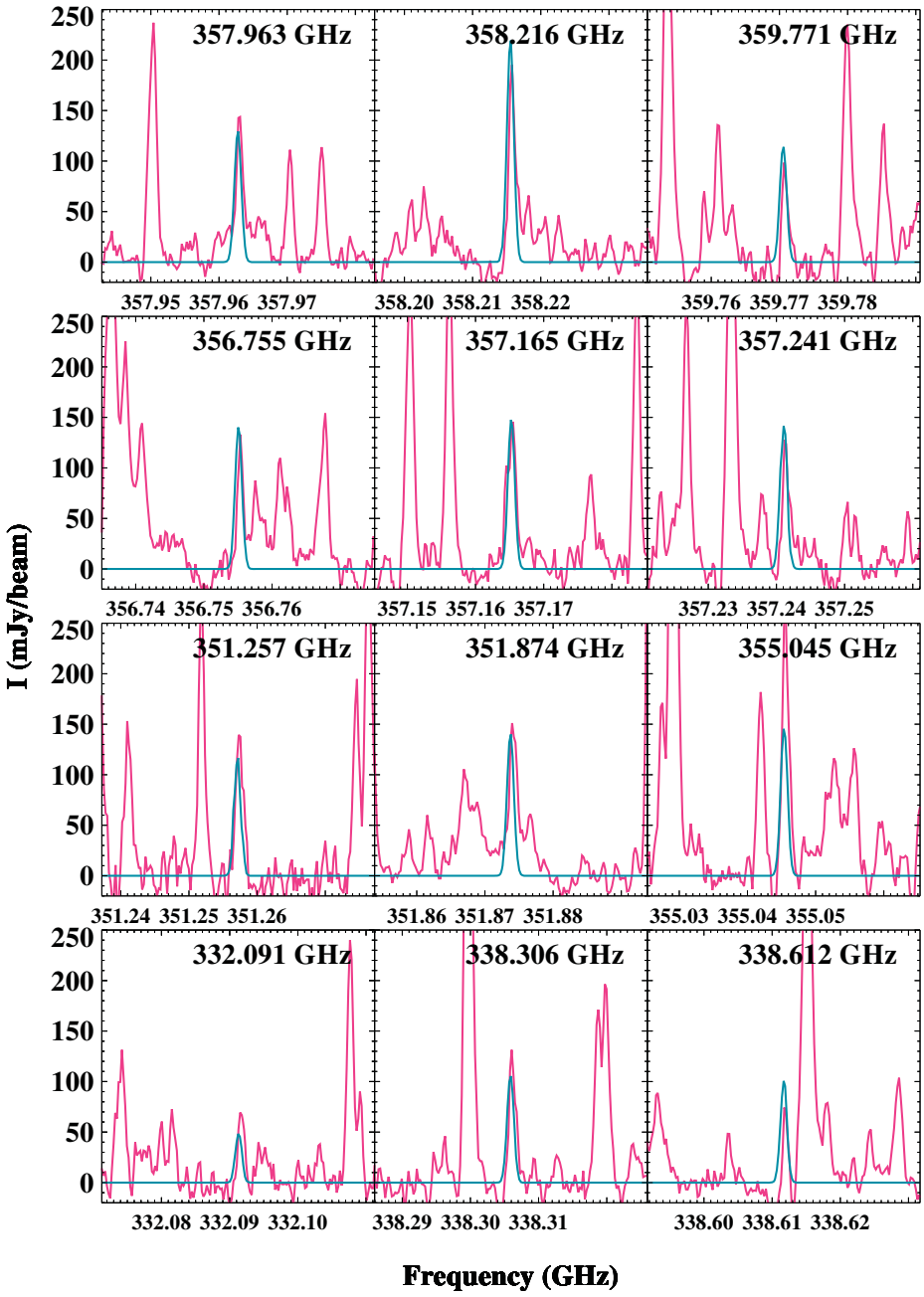

Figure 5.3: Twelve selected lines of SO_2 in the $v = 0$ state.

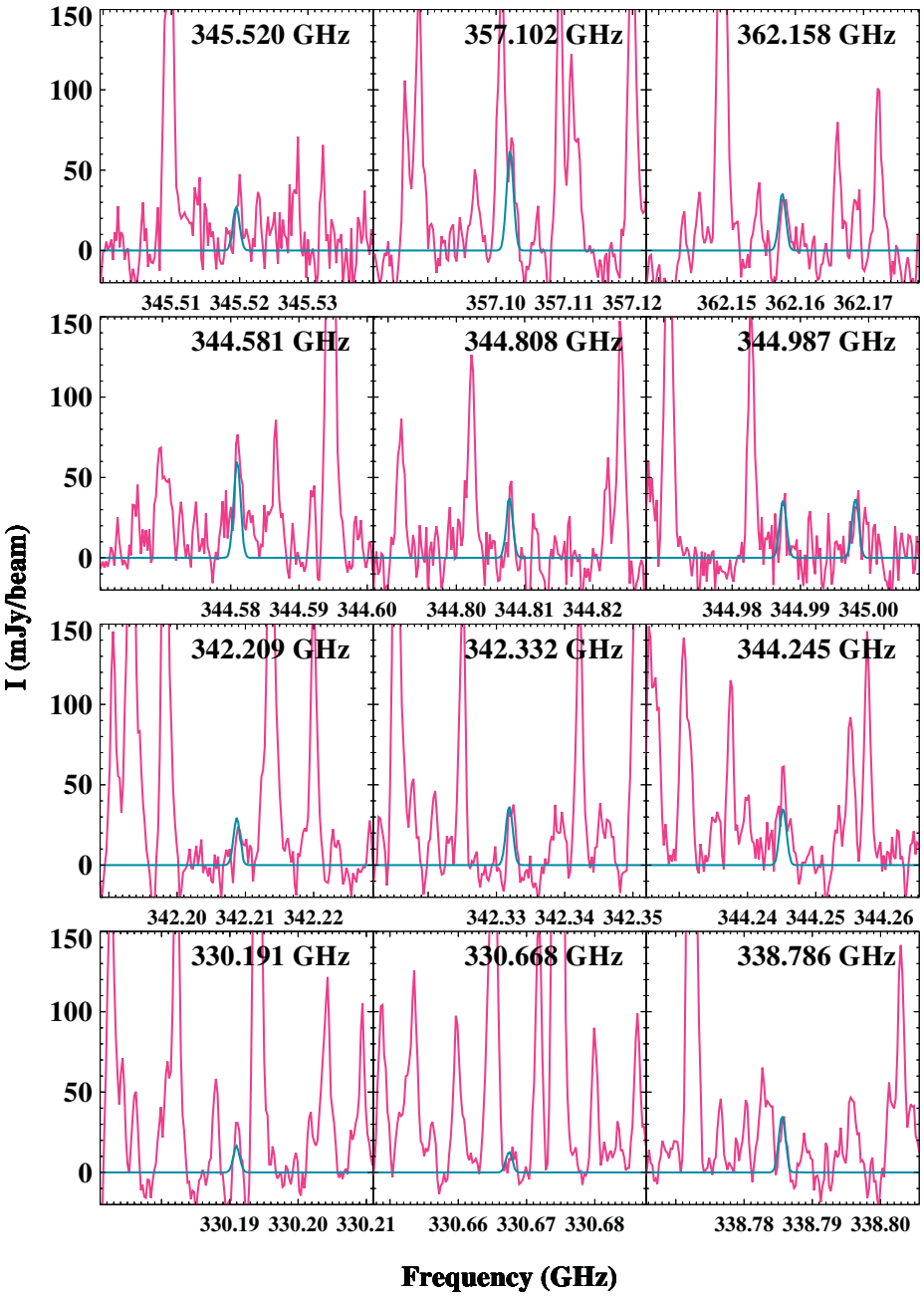

Figure 5.4: Twelve selected lines of $^{34}SO_2$.

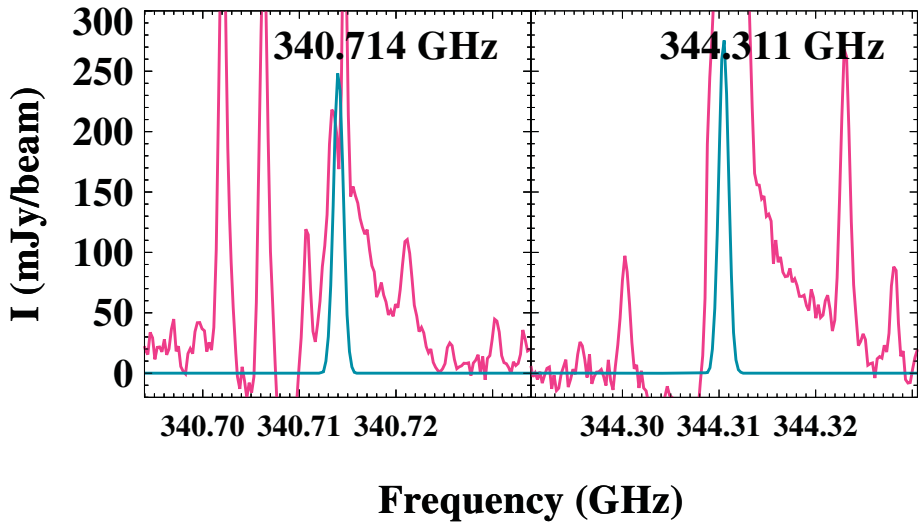

Figure 5.5: Two selected lines of SO in the $v = 0$ state.

SPECTROSCOPIC LABORATORY INFORMATION

The database sources, CDMS or JPL catalogs with their entry numbers, have been provided in the main text for all the species that we have searched for. In addition, the primary references on which these entries are based along with references for the dipole moments for all detected or possibly detected species are given below. Furthermore, the references with laboratory measurements in the range of our survey in cases in which the primary reference does not cover such data or if these data are an important contribution to the line list are also included.

SO_2

The $v = 0$ and $v_2 = 1$ entries for the main isotopic species are based on Müller and Brünken, (2005), those for $^{34}SO_2$ - on Belov et al., (1998). The dipole moment of SO_2 in several vibrational states was determined by Patel et al., (1979).

SO

The SO entry is based on Bogey et al., (1997). Its dipole moment was measured by Powell and Lide, (1964).

OCS

The main sources for the OCS entries are Golubiatnikov et al., (2005) (OCS, $v = 0$), Morino et al., (2000) (OCS, $v_2 = 1$), Dubrulle et al., (1980) ($O^{13}CS$, $OC^{34}S$, $OC^{33}S$). Dipole moment values were determined for OCS in various vibrational states and for several isotopic species by Tanaka et al., (1985).

CS

The CS entries are based on Müller et al., (2005), and the main sources of laboratory data are Bogey et al., (1982) and Ahrens and Winnewisser, (1999). The dipole moments of CS in $v = 0$ and 1 were measured by Winnewisser and Cook, (1968).

H_2CS

The H_2CS data are largely from Maeda et al., (2008), those of HDCS are from Minowa et al., (1997). Fabricant et al., (1977) determined the dipole moment of H_2CS.

H_2S

The H_2S entry is based to a considerable extent on Belov et al., (1995). The entries of HDS and $HD^{34}S$ are based on Camy-Peyret et al., (1985). The HDS transition frequencies with microwave accuracy were summarized by Helminger et al., (1971). Hillger and Strandberg, (1951) reported a small number of $HD^{34}S$ and HDS transition frequencies. Viswanathan and Dyke, (1984) determined dipole moments of H_2S, HDS and D_2S.

CH_3SH

The methyl mercaptan (methanethiol) entry is based on Xu et al., (2012) with transition frequencies in the range of our survey from Bettens et al., (1999). The information on the dipole moment components was provided by Tsunekawa et al., (1989).